PHYSICAL REVIEW B VOLUME 55, NUMBER 1 1 JANUARY 1997-I

Development of a semiempirical *n*-body noncentral potential for Fe-Al alloys

R. Besson*
*Centre Science des Matériaux et des Structures, URA CNRS 1884, Ecole des Mines de Saint-Etienne,
42100 Saint-Etienne CEDEX 9, France*

J. Morillo
*Laboratoire des Solides Irradiés, Commissariat à l'Energie Atomique–Centre d'Etudes et de Recherhe sur les Materiaux,
URA CNRS 1380, Ecole Polytechnique, 91128 Palaiseau CEDEX, France*

(Received 1 August 1996; revised manuscript received 16 September 1996)

A semiempirical embedded-atom method potential including a noncentral additive term is derived for $\mathrm{Fe}_x\mathrm{Al}_{1-x}$ ($x \geqslant 0.5$) systems and extensively tested on bulk and defect $T=0$ K properties as well as temperature-dependent properties. Although particular attention is given to the stoichiometric ordered $B2$ compound, this potential also leads to a realistic description of the $D0_3$ ordered phase. It constitutes a model appropriate to the calculation of the properties of extended defects in Fe-Al alloys. [S0163-1829(97)02001-8]

I. INTRODUCTION

Due to their appealing high-temperature and corrosion resistance properties, intermetallic alloys form the subject of an increasing amount of studies (for a recent review see, for example, Ref. 1). Nevertheless, their mechanical behavior is up to now not fully understood: in particular, their strong room temperature intergranular brittleness,[2] impairing their industrial use as structural materials, has neither been satisfactorily explained nor remedied. The case of FeAl which, in spite of a good specific stiffness, has remained seldom used and less thoroughly studied than its closest Ni-Al ($B2$ NiAl and $L1_2$ $\mathrm{Ni_3Al}$) ''neighbors,'' is however of interest because a more exhaustive comparison of the properties of both aluminides would help grasping the mechanisms of embrittlement. Moreover, the absence of reliable potentials for Fe-Al alloys has slowed down further headways in the knowledge of their atomic scale properties. Several works relying on pair potentials[3–7] have attempted to describe a few aspects of their behavior, but firmer physical bases are doubtlessly necessary, if complex phenomena such as segregation at grain boundaries and composition effects are to be tackled. The current deficiencies in this area urged us to elaborate a semiempirical potential realizing a compromise between a realistic account of physical properties and the need of preserving tractability in numerical calculations. In a preliminary study exposed elsewhere,[8] we briefly reported the fitting of this model as well as a few tests of its $T=0$ K behavior. The subject of the present paper is first to resume a more comprehensive description of the parameters that need to be taken into account in such a task, and secondly to give a more extensive dimension to the tests checking the validity of the model.

The Fe-Al system is described by such a complex phase diagram that it is totally hopeless to attempt to determine a potential whose reliability would extend over the whole range of compositions. Because $B2$ FeAl possesses hardly understood mechanical properties, and for purpose of future comparisons with $B2$ NiAl, we focused our attention on getting a satisfactory description of the characteristics of the $B2$ phase (this ordered phase, according to diffraction data,[9] exists between 38 and 52 at. % Al and is nearly perfect in a wide range of temperatures and concentrations). However, in order to be efficient in the study of segregation processes at interfaces, this description should also take into account pure elements. We therefore developed a unique model of potential for $\mathrm{Fe}_x\mathrm{Al}_{1-x}$ $(0.5 \leqslant x \leqslant 1)$, adjusted on static properties of pure bcc iron, pure fcc Al and $B2$ FeAl. Evaluation of the chemical potentials in the equiatomic $B2$ alloy at $T=0$ K yielding very good values (together with an acceptable agreement for chemical potentials in $D0_3$ $\mathrm{Fe_3Al}$), this model can reasonably be regarded as reliable for static simulations of pure Fe and Al as well as of alloy interfaces. Another outstanding point is its prediction of the negative Cauchy discrepancies of FeAl and $\mathrm{Fe_3Al}$, thus suggesting that the angular interactions (at least those in perfect cubic structures) are adequately taken into account. At nonzero temperatures, it also provides a reasonably good description of the $B2$ alloy thermal behavior, provided no large clusters of pure elements exist. The present paper is organized as follows. In Sec. II, we present the arguments guiding us in our choice of a definite functional form. In Sec. III, our results are presented and discussed, and Sec. IV concludes and presents perspectives for further works.

II. THE POTENTIAL

A. Arguments for choice

Due to their simplicity, pair potentials are well suited for generic studies of trends among a given class of metallic materials. However, as they do not account for mostly important many-body electronic effects in metallic systems, they cannot be relied on to properly describe the specific properties of such compounds. For more than a decade, the embedded-atom method[10] (EAM) and the second-moment approximation of the tight-binding scheme[11] (SMA) have been the two most common approaches leading to n-body central force potentials, able to overcome these major limi-

© 1997 The American Physical Society

tations. The physical basis of EAM models makes them valid, strictly speaking, for normal[12] or noble[13] metals (with an almost uniform electron density), whereas SMA is *a priori* well suited for transition elements[14] (d-band directional bonding). The formal expressions obtained in both cases being quite similar (SMA can be regarded as EAM restricted to a square root embedding function), they cannot be distinguished from a semiempirical point of view, which is conceptually quite satisfactory. However, this apparently unified description of metallic cohesion shows severe limits when the electronic density no longer can be regarded as quasiuniform because of bonds displaying a strongly directional character.[15] Although such a behavior is obviously the realm of semiconductors, bcc central transition metals (such as Fe, Cr) also characterized by high directional effects, represent a striking example of the failure of classical n-body central potentials when applied to metallic systems. In principle, only explicit angular interactions can faithfully reproduce the properties of these compounds. To obtain analytic approximate forms for such potentials (in which the energy of a particle no longer depends solely on its distance from the neighboring particles, but also on angles between neighbors), the most natural way is obviously to refine the moment analysis. It has been performed by several authors, within the frame of the tight-binding bond method.[16,17] Using this scheme, Carlsson[18] showed that the use of a matrix second moment (rather than a scalar one) leads to angular interactions, provided the system is not too strongly coordinated (the Slater-Koster parameters[19] already imply explicitly angular terms if the hopping is neither maximal, nor equal to zero). But the main procedure to get systematic angular interactions is to carry the development to an order higher than 2. In metals with a half-filled d band, the contribution of the third moment can be shown to be negligible.[15,20] Several models based on the fourth moment of the density of states have thus sometimes (although not systematically) led to an improvement in the description of atomic interactions, especially for defect properties.[15,21] However, the relatively high complexity of the corresponding expressions makes it worthwhile to try simpler (though less firmly justified theoretically) schemes. In almost all these cases, the key idea to describe n-body noncentral interactions (with $n \geqslant 3$) is to choose an expression that vanishes for the monocrystalline ground state and increases with increasing departure from this reference state. This approach was first used for semiconductors, the simplest triplet potential being written as

$$V_{ijk}=f(r_{ij})f(r_{ik})(\cos\theta_{jik}+1/3)^2, \tag{1}$$

so as to favor 109° tetrahedral bonds.[22] A more rigorous generalization was carried out by expanding the angular dependence on Legendre polynomials.[23] An alternative procedure involves an additional three-body noncentral term introduced as an angularly dependent correction for the density over a site,[24,25] the angular part of which reads $\cos^2\theta_{jik}-1/3$. This second form, stabilizing cubic bonds, was later derived by Pasianot and co-workers[26] on purely empirical grounds, so as to mimic the Kanzaki dipole tensor associated with each particle.[27] The expression they obtained is very simple, the angular dependence appearing as a third additive term. Classical EAM forces need just be augmented by this third noncentral term, without any modification in the embedding and pairwise parts. This functional form proved quite successful in modeling transition metals known to be very poorly described in classical frames (Nb, Fe, Cr). For aluminum, the situation is rather different: this metal has been the subject of investigations aiming at deriving EAM potentials (see, for example, Ref. 12), but contrary to early expectations, it hardly lends itself to classical n-body descriptions: its high free electron density makes it necessary to take into account many shells of neighbors, especially when the configuration is highly disrupted with respect to the perfect crystal.

Apart from the above quoted restrictions, EAM-like expressions remain intuitively satisfactory and have thus been largely used to model multicomponent systems, initially consisting of fcc metals,[28–30] and more recently involving bcc structures.[31] Ni_3Al first and more recently NiAl (two examples quite close to the one examined in this paper) have been successfully modeled by several authors[32–34] using various EAM schemes, whereas no semiempirical work has been carried out on iron-rich Fe-Al systems. Previous band structure calculations[35–37] agree that the cohesion between Al and Fe involves a strong sp-sd hybridization responsible for directional bonds, as illustrated by a negative Cauchy discrepancy $C_{12}-C_{44}$, a mathematical condition that can simply not be accounted for by EAM or SMA potentials.[38] Contrary to a lot of other intermetallic alloys lending themselves to systematic studies (for example Refs. 39 and 40), $B2$ and $D0_3$ Fe-Al have been studied by first principles calculations only by few authors.[35–37] As a consequence, the absence of data concerning the relative energies of crystalline structures makes it uneasy to perform a semiempirical fit on reliable bases: the classical procedure, in which energy differences are explicitly imposed so as to make it sure that the most stable calculated structure will correspond to the one observed experimentally, cannot be followed here. The most reassuring attitude would be to derive an analytic expression on a theoretically firm basis, as did Moriarty[41] for central transition metals (model generalized pseudopotential theory). But such potentials are too complex to be used in classical molecular dynamics and Monte Carlo calculations of large systems such as grain boundaries.

Contrary to pure central transition metals, Fe-Al alloys involve a normal metal whose effect should be to modify the density of states sensibly, in such a way that the third moment of the DOS no longer be negligible (according to *ab initio* calculations,[36,42] the d band deviates from half-filling in such cases). This provides an *a priori* justification for truncation of the development to three-body interactions, namely one order below that used for unalloyed transition elements. In this framework, the analysis of the authors of Ref. 26 seems particularly well suited. Their procedure can be viewed as a generalization of classical EAM which, due to the larger number of degrees of freedom available in EAM than in SMA,[38] has constituted the basis of the majority of previous works on alloys.

B. Analytic form

We thus write the energy of an assembly of atoms of both Al and Fe types as

$$E=\sum_{i\in I_{\mathrm{Al}}}\left[F_{\mathrm{Al}}(\rho_i)+\frac{1}{2}\sum_{\substack{j\neq i\\ j\in I_{\mathrm{Al}}}}V_{\mathrm{AlAl}}(r_{ij})+\alpha_{\mathrm{Al}}Y_i^2\right]+\sum_{i\in I_{\mathrm{Fe}}}\left[F_{\mathrm{Fe}}(\rho_i)+\frac{1}{2}\sum_{\substack{j\neq i\\ j\in I_{\mathrm{Fe}}}}V_{\mathrm{FeFe}}(r_{ij})+\alpha_{\mathrm{Fe}}Y_i^2\right]+\sum_{\substack{i,j\neq i\\ i\in I_{\mathrm{Al}}\\ j\in I_{\mathrm{Fe}}}}V_{\mathrm{FeAl}}(r_{ij}), \tag{2}$$

where

$$\rho_i=\sum_{j\neq i} f_j(r_{ij}) \tag{3}$$

and I_{Al} (resp. I_{Fe}) stands for the set of indices of Al (resp. Fe) atoms.

F_i and f_i are respectively the embedding and electronic density functions of atom i, ρ_i is the induced density over site i, V_{ij} is a pair potential classically collecting elsewhere ill-described interactions (exchange and correlation, electron core repulsion, etc.), and $\alpha_i Y_i^2$ is the noncentral term.

1. Pair potentials

In dilute disordered alloys of noble or transition metals, a simple approximation of cross interactions with geometric or arithmetic means of those of pure elements has proved to be a reliable procedure in many cases. But this approach no longer holds in systems governed by less homogeneous interactions, and cross potentials must be treated exactly in the same way as other terms. Thus a unique expression was assumed for each of the three pair interactions (k=Al-Al, Fe-Fe, or Al-Fe):

$$V_k(r)=\psi_k(r)-\psi_k(D_{p,k})+\frac{D_{p,k}}{20}\left[1-\left(\frac{r}{D_{p,k}}\right)^{20}\right]\psi_k'(D_{p,k}) \quad \text{for } r<D_{p,k}. \tag{4}$$

The only purpose of this complex form is to ensure that the function goes continuously to zero at the cutoff adjustable distance $D_{p,k}$;

$$\psi_k(r)=\psi_{0,k}[\exp(-2\gamma_k(r-t_k))-2\exp(-\gamma_k(r-t_k))] \tag{5}$$

is a Morse function containing three free parameters t_k, γ_k, and ψ_k. Our choice was guided by a seek for compromise between simplicity and generality: this very flexible function covers purely repulsive as well as short-distance attractive interactions.

2. Density functions

We chose simple exponential forms, reflecting the main radial dependence of free atom electronic densities:

$$f_k(r)=f_{0,k}\exp\left[-\beta_k\left(\frac{r}{a_{0,k}}-1\right)\right], \tag{6}$$

where $a_{0,k}$ is the equilibrium first-neighbor distance of the element, $f_{0,k}$ and β_k being adjustable parameters (k=Al or Fe).

Contrary to pair potentials, density functions are cut to zero at a distance $D_{d,k}$ fixed prior to any fitting procedure, but possibly increased if the resulting discontinuity at this cutoff distance is not negligible.

3. Embedding functions

The embedding functions, involving the four adjustable parameters A_k, $F_{0,k}$, $F'_{0,k}$, $F''_{0,k}$ for each species (k=Fe or Al), are

$$F_k(\rho)=\frac{A_k}{2\rho}+\frac{[(\rho_{0,k})^4F''_{0,k}-A\rho_{0,k}]}{6\rho^2}+\left[F'_{0,k}+\frac{A_k}{6(\rho_{0,k})^2}+\rho_{0,k}F''_{0,k}/3\right]\rho+F_{0,k}-\rho_{0,k}F'_{0,k}-(\rho_{0,k})^2F''_{0,k}/2-\frac{A_k}{2\rho_{0,k}} \tag{7a}$$

if $\rho>\rho_{0,k}$,

$$F_k(\rho)=\rho^2F''_{0,k}/2-[F'_{0,k}-\rho_{0,k}F''_{0,k}]\rho+[F_{0,k}-\rho_{0,k}F'_{0,k}+F''_{0,k}(\rho_{0,k})^2/2]\left[1+\left(\frac{\rho}{\rho_{0,k}}-1\right)^3\right] \tag{7b}$$

otherwise.

They were designed to have the following properties:

$$F(0)=0, \quad F^{(p)}(\rho_0)=F_0^{(p)} \quad (p=0,1,2) \tag{7c}$$

(ρ_0 is the density over a monocrystalline site of pure element at equilibrium, fixed by the density functions). Moreover, the physically significant property of positive curvature (which corresponds to the weakening of successive bonds) is automatically satisfied for $\rho>\rho_0$; if $\rho<\rho_0$, it depends on F_0, F'_0, F''_0 and has to be checked *a posteriori*.

The parameter A governs the slope for strong densities. It has no effect on the fitting process of pure metals because all the densities considered here are lower than the equilibrium value, but it modifies the energies of defects involving high densities.

4. Noncentral interactions

The noncentral interaction terms $\alpha_i Y_i^2$ (i=Fe or Al) are supposed to contain all that information about directionality which is not taken into account by the first two classical terms. It depends linearly on a unique parameter α_i governing its global intensity.

Initially,[26] Y_i^2 was defined as the second invariant of a tensor $\bar{\bar{\lambda}}_{\mathrm{i}}$:

$$\lambda_i^{\alpha\beta}=\sum_{j\neq i} f_j(r_{ij})\,\frac{(r_j^\alpha-r_i^\alpha)(r_j^\beta-r_i^\beta)}{(r_{ij})^2} \tag{8a}$$

which, recast to yield a more explicit three-body expression, reads as follows:

TABLE I. Values of parameters for Fe, Al, and FeAl interatomic potentials (units: eV and Å).

	Pure elements		FeAl alloy		
	Al	Fe	Al	FeAl	Fe
f_0	10^{-3}	10^{-3}	10^{-3}		9.21×10^{-4}
β	5.8	6.0			
γ	0.3	0.9		0.35	
t	3.45	2.8		2.5	
ψ_0	0.8663	1.3152		0.961	
A	0.8	0.08			
y			-7.42		-84.35
α	89	1992	7467		108064
F_0	-1.46	-3.6			
F_0'	68.2	-144.6			
F_0''	4647.0	2866.9			
ρ_0	1.289×10^{-2}	9.80×10^{-3}			
ρ_{B2}			1.333×10^{-2}		1.878×10^{-2}
D_p	5.65	3.5		4.4	
D_d	5.4	4.4			

$$Y_i^2=\sum_{\substack{j\neq i\\ k\neq i}} f_j(r_{ij})f_k(r_{ik})\left(\cos^2\theta_{jik}-\frac{1}{3}\right). \tag{8b}$$

Density functions ensure the physically essential feature that angular interactions must vanish when bond lengths are increased at constant angles.

C. Fitting procedure

1. Pure metals

In an EAM potential for a pure metal, f_0 acts only as a scaling parameter: for fixed t, γ, ψ, D_p, β, and F_0, varying f_0 at constant f_0F_0', $(f_0)^2F_0''$, $(f_0)^2\alpha$, and A/f_0 generates a class of physically equivalent models. The value of f_0 was thus settled arbitrarily to 10^{-3} for both Fe and Al. The potential for each of pure metals depends on the following 10 effective parameters: t, γ, D_p, β, A/f_0, F_0, f_0F_0', $(f_0)^2F_0''$, ψ, and $(f_0)^2\alpha$. The linear dependence of the five equations expressing the five basic bulk $T=0$ K properties (sublimation energy, lattice parameter, and the three elastic constants) upon the last five parameters made it possible to calculate them so as to reproduce exactly those properties. We obtained a class of potentials still parametric with respect to t, γ, D_p, β, and A/f_0, among which we selected the one yielding the best values for the relaxed vacancy formation energy and (001) surface energy.

2. B2 alloy

To get the alloy potential, we made use of two usual properties of the EAM energy of monatomic crystals: first, subtraction of any linear function $y\rho$ (y constant) from the immersion function $F(\rho)$ of an element does not modify the configurational energy, provided this operation is balanced with the addition of $2yf$ to the corresponding pair potential, and secondly, for a binary alloy, only $f_0^{\mathrm{Al}}/f_0^{\mathrm{Fe}}$ has a physical meaning[38] (quite similarly to the case of a single element, variation of one of the f_0's at constant ratio generates equivalent models). The corresponding three additional degrees of freedom (y_{Al}, y_{Fe}, and $f_0^{\mathrm{Al}}/f_0^{\mathrm{Fe}}$) can be exploited to explore a wider part of the space of parameters.

f_0^{Al} was thus kept equal to 10^{-3} and f_0^{Fe} subsequently calculated. In the alloy, the values of t, γ, ψ, D_p relative to the cross interaction, the ratio $f_0^{\mathrm{Al}}/f_0^{\mathrm{Fe}}$, the scaling parameters y_{Al}, y_{Fe} and two modified values (one for each element) of the angular parameters α were to be determined, namely nine free parameters. Among these, the five basic monocrystalline properties of the perfect $B2$ phase could be exactly reproduced by linearly solving for ψ_{FeAl}, y_{Al}, y_{Fe}, α_{Al}, and α_{Fe} (the last two parameters having new values characterizing the $B2$ atomic environment), therefore leaving four free parameters ($t,\gamma,f_0^{\mathrm{Al}}/f_0^{\mathrm{Fe}},D_p$) whose values were settled by fitting the $1/2[111](1\bar{1}0)$ $B2$ antiphase boundary energy.

Finally, it should be noted that in lattices with a base, calculation of the elastic constants can generally not be performed analytically, since a homogeneous deformation leads to an unrelaxed nonphysical state. However, the particular symmetry of the $B2$ structure enables such an analytical evaluation.

III. RESULTS

A. Potentials

Table I displays the optimized values of parameters in our model and Table II gives the values of the five basic properties on which all fittings were performed. The maximum interaction cutoff distances of 4.4 (density function for Fe) and 5.65 Å (pair interaction for Al) correspond to taking into account three shells of neighbors for the descriptions of Fe and Al. Concerning density functions, the decrease of the density induced by Fe is more rapid than that of Al, hence a cutoff distance larger for Al than for Fe. However, on account of the difference in lattice parameters, this corresponds

TABLE II. Values of $T=0$ K properties on which the fit was performed. Energies in eV/atom for pure elements, in eV/(pair Al +Fe) for $B2$ FeAl; lattice parameters in Å; elastic constants in 10^{12} dyn/cm^2. While all values for pure elements were taken from experiments, *ab initio* calculated values were thought to be a more acceptable reference for FeAl (to insist on the strong temperature dependence, values corresponding to 300 K are also displayed between parentheses, together with relative thermal variations).

	Al	Fe	$B2$ FeAl	
Cohesive energy	3.34[a]	4.29[a]	8.15[b]	
Lattice parameter	4.04[c]	2.86[c]	2.90[d]	
C_{11}	1.14[e]	2.33[e]	2.90[d] (1.81[e])	**−37%**
C_{12}	0.62[e]	1.35[e]	1.30[d] (1.14[e])	**−12%**
C_{44}	0.32[e]	1.17[e]	1.65[d] (1.27[e])	**−23%**
$C_{12}-C_{44}$	0.30	0.18	−0.35 (−0.13)	**63%**

[a] Reference 43.

[b] Reference 44.

[c] Reference 45.

[d] Reference 35, first-principle calculation.

[e] Reference 46.

to the same number of neighbor shells. By contrast, in the $B2$ compound, the range of Al-induced interactions reaches the fifth neighbor shell, namely two lattice parameters. It can interestingly be noted that the first neighbor Al-Al distance is approximately the same in pure Al and in $B2$ FeAl (2.85 vs 2.9 Å), whereas in this alloy, the closest Fe-Fe pairs are at the same distance as second neighbors in pure Fe. At equilibrium, the immersion contributions to cohesion are smaller (absolute values) than cohesive energies, and therefore pair interactions in these models are attractive. However, as explained precedently, because of the multiple formulations of potentials for pure elements, this feature has no physical meaning: in a pure metal, the pair interaction can (to a certain extent) be made arbitrarily positive or negative, according to the imposed shape of the immersion part. In alloys, on the other hand, performing the fitting procedure removes this degree of freedom and, provided the picture of EAM is accepted as valid, the attractive character of pair interactions can no longer be regarded as fortuitous. In $B2$ FeAl, the contribution of the (Al) third shell of neighbors of an Al atom to the chemical potential of this atom roughly amounts to -1 eV (see Table III). This ''long-range'' interaction between Al atoms in $B2$ FeAl is characteristic of the behaviour of Al, known to induce long-range perturbations.

B. Pure elements properties

1. Crystallographic structures and T=0 K equations of state

We checked the validity of pure element potentials by comparing the relative stabilities of the bcc, fcc, and hcp structures. Without including this constraint in the fitting procedure, the fcc and bcc structures are found to be the most stable ones respectively for Al and Fe at $T=0$ K (see Table II of Ref. 8). We also compared the 0 K bulk behavior of our models to the universal equation of state in reduced units proposed by Rose *et al.* (Ref. 47):

TABLE III. Energetic contributions (eV) of the successive neighbor shells to the pair cohesive energies of Al and Fe atoms in $B2$ FeAl. D and I respectively stand for different and identical types of atoms (with respect to the one considered).

Shell number	Al	Fe
1 (D)	−0.70	−0.70
2 (I)	−0.45	−0.6
3 (I)	**−1.00**	−0.05
4 (D)	≈0	≈0

$$E^*=-(1+a^*)\exp(-a^*), \quad E^*=E/E_{\mathrm{coh}},$$

$$a^*=(r_{\mathrm{WS}}-r_{\mathrm{WSe}})(12\pi B r_{\mathrm{WSe}}/E_{\mathrm{coh}})^{1/2}, \tag{9}$$

with B the bulk modulus, r_{WS} and r_{WSe} the current and equilibrium values of the Wigner-Seitz radius, and E_{coh} the cohesive energy. None of our two models follows this equation of state on the whole range of lattice parameters. However, the simulated Fe and Al behave in quite dissimilar ways. The behavior of Al under negative pressures (expanded lattice: $a^*>0$) shows reasonable agreement with Ref. 47, whereas at high pressures ($a^*<0$), the repulsive interaction is overrated. On the other hand, the Fe model is realistic under high pressures but suffers from a very fast loss of cohesion when the volume is raised over its equilibrium value. Since a correct fitting to the Rose equation had not been included in the data base (reasons for this choice are given below), such deviations are not surprising.

2. Point defects and (100) surfaces

The energies of all relaxed structures were evaluated with a molecular dynamics (MD) program used according to the quasidynamical method.[48] Detailed values are reported in Table I of Ref. 8. On the whole, the agreement with experimentally measured energies (Ref. 14 for Fe, Refs. 12 and 49, respectively, for vacancy and surface in Al) is excellent. As said previously, obtaining realistic values for these properties needed an additional fit, due to the nonuniqueness of the solutions to the equations involving only cohesive energies, lattice parameters, and elastic constants. However, within the constraints of valid defect energies, the solution seems to be unique. Our functional forms of potentials thus easily ''accept'' to reproduce static properties of defects. The flexibility of Morse functions is probably responsible for this adequacy.

3. Phonon spectra

For the calculation of the dispersion curves and density of states, the force constants matrices were calculated by numerical evaluation of the second derivatives of energy for incremental displacements of the reference atom and of its neighbors along all possible couples of directions, according to the formulas

$$D_{ii}^{\alpha\alpha}=\frac{E(R_i^{\alpha}+\varepsilon)+E(R_i^{\alpha}-\varepsilon)-2E(R_i^{\alpha})}{\varepsilon^2}, \tag{10a}$$

$$D_{ij}^{\alpha\beta}=\frac{1}{2}\left[\frac{E(R_i^{\alpha}+\varepsilon,R_j^{\beta}+\varepsilon)+E(R_i^{\alpha}-\varepsilon,R_j^{\beta}-\varepsilon)-2E(R_i^{\alpha})}{\varepsilon^2}-D_{ii}^{\alpha\alpha}-D_{jj}^{\beta\beta}\right], \tag{10b}$$

where E is the potential energy and R_i^{α} the α component of the position of atom i, with ϵ equal to 10^{-4} in a double precision calculation.

As displayed on Fig. 1, the overall shapes of phonon spectra are correctly predicted, mostly for Fe. Low wave vector frequencies always show excellent agreement with experiment, because they directly reflect elastic constants, which are exactly reproduced in our model. As regards other points of the reciprocal space, the analytic form of the potential seems to be better suited for Fe than for Al. In Al, the zone edge frequencies are globally underestimated by 25%, whereas in the case of Fe, they are underestimated by less than 10%, particularly along $[\zeta\zeta\zeta]$ and $[\zeta\zeta 1]$ directions. As for densities of vibrational states, the agreement is satisfactory between our calculations and analytic models (Ref. 51) in Fe. In Al, however, we obtain a global lowering of the spectrum,[52] together with an exaggerated contribution of medium frequencies reflecting the poor reproduction of zone edge behavior.

4. Thermal expansion and mean-square displacements (MSD)

Lattice expansion is a good indicator of the behavior of the model for nonzero temperatures. To assess this property, we used a standard constant temperature and pressure MD algorithm.[53] The models for Fe and Al prove to be very different: the calculated lattice expansion of aluminum is close to experiments,[43,46] whereas for Fe it is twice lower than the measured values,[43,54] as shown in Table IV (first and second columns). On the other hand, the mean-square displacements (Fig. 2) behave in a reverse way: the agreement with experiment is reasonable for Fe, but the amplitude of Al atoms displacements is too large, which results in a melting-point underestimated by 30% for the latter element (bulk $T_m=550$ K according to the discontinuity in lattice parameters). By comparison, Fe exhibits a more classical behavior in molecular dynamics simulations, its calculated bulk melting point ($T_m=2100$ K) being over the experimental one by 10%, a reasonable overestimated value due to the absence of surfaces.

It is interesting to compare the experimental and MD simulation MSD to those obtained in the harmonic and quasiharmonic approximations, given by the following expression:

$$\langle u^2\rangle=\frac{3\hbar}{2m}\int_0^{\omega_{\max}}\frac{g(\omega)}{\omega}\coth\left[\frac{\hbar\omega}{2k_BT}\right]d\omega, \tag{11}$$

where the quasiharmonic correction amounts to replacing the 0 K density of states with that calculated for the mean lattice parameter at the studied temperature.

The MSD obtained in these approximations are also shown in Fig. 2. In the case of Al, it can be seen that the experimental MSD are overestimated by our model for the following two reasons: (i) the shift of our model density of states towards lower frequencies and (ii) very large anharmonic effects right from low temperatures (300 K), which cannot be taken into account by the simple quasiharmonic approximation. This means that anharmonic effects cannot be neglected in our potential for Al, even at low temperatures. By contrast, in the case of Fe, the agreement between the experimentally measured MSD, the MD simulation result and the various models is excellent, especially if one considers the large dispersion in experimental data. Thus anharmonicity should represent only a first order effect in the Fe potential.

For a given element, properties such as $T=0$ K equation of state, phonon spectrum and dynamic behavior are known to be highly dependent on one another. First, a good agreement with the Rose universal equation of state is sometimes considered as a guarantee for an acceptable thermal expansion. Following this point of view, the present work embodies a striking example, since it is very appealing to correlate the correctly (resp. poorly) reproduced thermal expansion of Al (Fe) to the agreement (disagreement) with the Rose curve for lattice parameters higher than the equilibrium value in the accessible experimental range $[a^*(T_m)=0.1$ for Al and 0.02 for Fe$]$. To assess more precisely the role of the $T=0$ K equation of state in the thermal behavior, we thus modified our embedding functions so as to include the Rose curves in our data base (the density functions and pair potentials being unchanged, all equilibrium properties were preserved in this transformation). The corresponding new values of thermal expansions are listed in Table IV (third column), together with that of the main model. From these figures, it is clear that thoroughly reproducing the 0 K equation of state cannot be considered as a sufficient condition to obtain a realistic thermal behavior since, in spite of an improvement in the behavior of Fe, the disagreement with experimental data becomes more pronounced for Al.

Finally, one can try to estimate the true (surface-dependent) melting point of the pure Al and Fe models by use of the well known Lindemann criterion,[57] which states that fusion occurs when the root mean-square displacement reaches a critical fraction δ_m of the nearest-neighbor distance d_1. Assuming that the models are characterized by the same value $\delta_m^{\exp}$ of the Lindemann parameter as the corresponding real systems, the true melting temperature of the model T_m^{model} is given by

$$\frac{\sqrt{\langle u^2(T_m^{\text{model}})\rangle^{\text{model}}}}{d_1(T_m^{\text{model}})}=\delta_m^{\exp}. \tag{12}$$

The Lindemann parameters for Al and Fe at fusion being respectively 0.072 (Ref. 58) and 0.0787,[59] the estimated

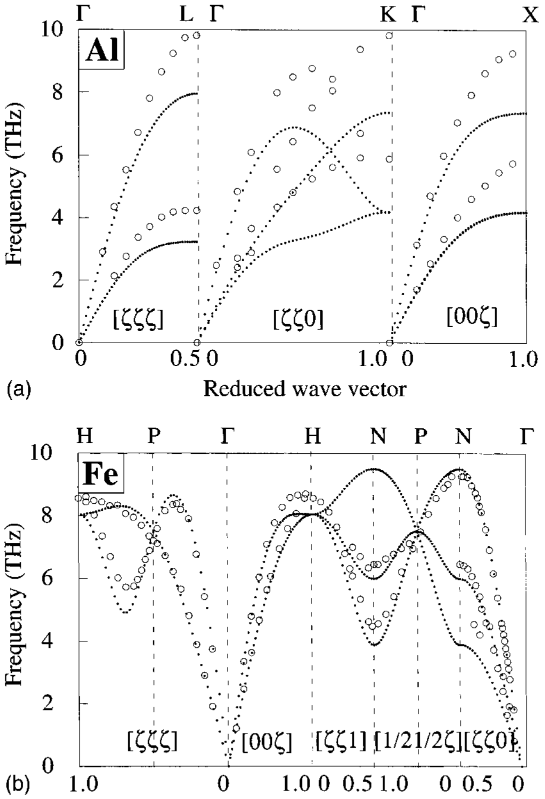

FIG. 1. Dispersion relations (a) for Al and (b) for Fe. Open circles correspond to experimental data (Refs. 50 for Al and 51 for Fe).

melting temperatures amount to 450 and 1900 K, two values slightly lower (between 15 and 20%) than those found by direct examination of the discontinuity on the calculated thermal expansion curves.

C. Alloys properties

1. B2 properties

a. Stability of the structure. We checked this property by comparison with the $B32$ ($cF16$, NaTl-type) bcc-based AB ordered structure. The latter being found to have an energy per atom pair equal to -8.06 eV (which corresponds to an energy increase equal to 0.1 eV/pair with respect to that of the $B2$ phase), the $B2$ phase is thus found to be stable relative to the $B32$. The $B2$ heat of formation amounts to 0.52 eV/pair, which is much larger than the $B2/B32$ difference and seems to be a relatively reasonable value compared to that obtained by *ab initio* calculations for other systems (typical values of 0.1 eV/atom were found by several authors reported in Ref. 60).

TABLE IV. Influence of the choice of immersion functions F on the linear thermal expansion coefficients of pure Al and Fe (ppm/K).

	Experimental values	Empirical F	Implicit F
Al	23.6[a]	21.2	3.0
Fe	11.7[a]	6.0	7.4

[a] Reference 43.

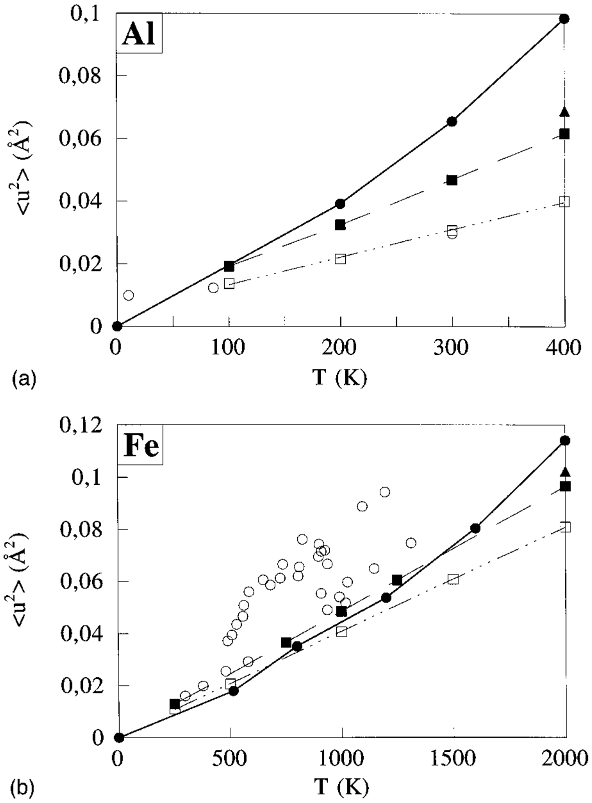

FIG. 2. Mean-square displacements for (a) Al and (b) Fe. Experiment (open circles), MD simulations (full circles), and harmonic approximation (our model: full squares; experiment: open squares; Refs. 55 for Al and 56 for Fe). The triangle represents one high temperature point in the quasiharmonic approximation of our model.

b. Phonon spectrum. The calculated dispersion relations for $B2$ FeAl shown in Fig. 3(a) cannot be directly compared to experiment, because the latter was measured on a compound containing only 25% Al.[61] However, the maximum frequencies, lower than in the case of pure Fe, are correctly predicted. The ''softening'' effect of Al is also restituted. A small frequency gap between optical and acoustic branches appears at point P, the magnitude of which is equal to 0.3 THz. As regards the density of states [Fig. 3(b)], alloying of Fe and Al atoms increases the contribution of low frequencies (around 5 THz).

c. Thermal expansion and MSD. $B2$ FeAl results are presented on Fig. 4. Our model proves to be satisfactory as concerns lattice expansion; experimental values are not available for mean-square displacements. The main feature is the larger amplitude of Fe vibrations compared to those of Al atoms (almost twice at 1600 K), in spite of the much larger mass of Fe atoms. This property seems to be related to the larger extent of the Al-Al interactions compared to Fe-Fe ones (as suggested by the force constants matrices between identical species). Size measurements of quenched-in and annealed samples of Fe 40 at. % Al (Ref. 63) have demonstrated that off-stoichiometric alloys possess up to 0.2% vacancies at elevated temperatures. However, the perfectly equiatomic compound exhibits lower amounts of defects at high temperatures (inferior to 0.1% up to 1300 K as explained below in point-defect considerations). Since the as-

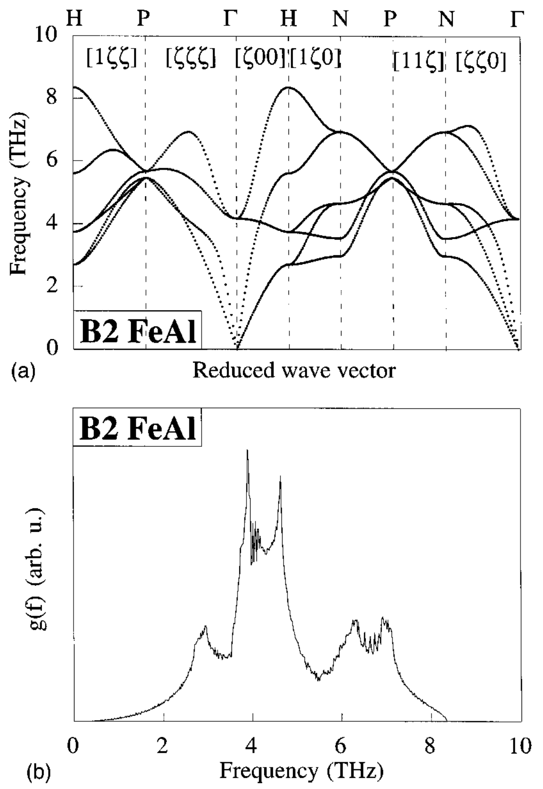

FIG. 3. (a) Dispersion relation and (b) density of states in $B2$ FeAl. The Brillouin zone is simple cubic.

sociated relaxation volume per defect does not exceed a few percent of the atomic volume, the resulting correction upon the thermal lattice parameter is of the order of 0.01%, thus negligible. By contrast, defects have a strong influence on melting, together with surfaces. One might thus expect to obtain a lower melting point by taking into account the state of disorder of the crystal. To check this point, a complete grand canonical Monte Carlo calculation at constant pressure must be performed, but this kind of simulation being extremely heavy (the algorithm enabling any atomic transition is very complex, and the cell should be quite large to remain physically meaningful up to the melting point), it has not been performed.

An upper bound for the ''true'' melting temperature of our model potential (with surfaces) is given by the MD bulk melting temperature of this model [Fig. 4(a)], $T_m = 2200$ K, a rather high value compared to the 1600 K measured experimentally. On the other hand, due to the very different magnitudes of MSD undergone by both species, applying some kind of Lindemann criterion to $B2$ FeAl is not as easy as in the case of pure metals to get a more precise estimation of T_m. Owing to the bcc ironlike structure of $B2$ FeAl (strongly conditioned by the properties of pure Fe, especially as for the structure and lattice parameter), it is reasonable to admit that the $B2$ critical Lindemann parameter has a value close to that of bcc iron, namely ≈0.08. The following estimated melting temperatures are then obtained: 1400 K with Fe MSD, 1900 K with Al MSD, and 1650 K with the mean MSD value. Thus the ''true'' melting temperature of our model potential lies certainly between 1400 and 2200 K, a reasonable frame compared to the experimental value.

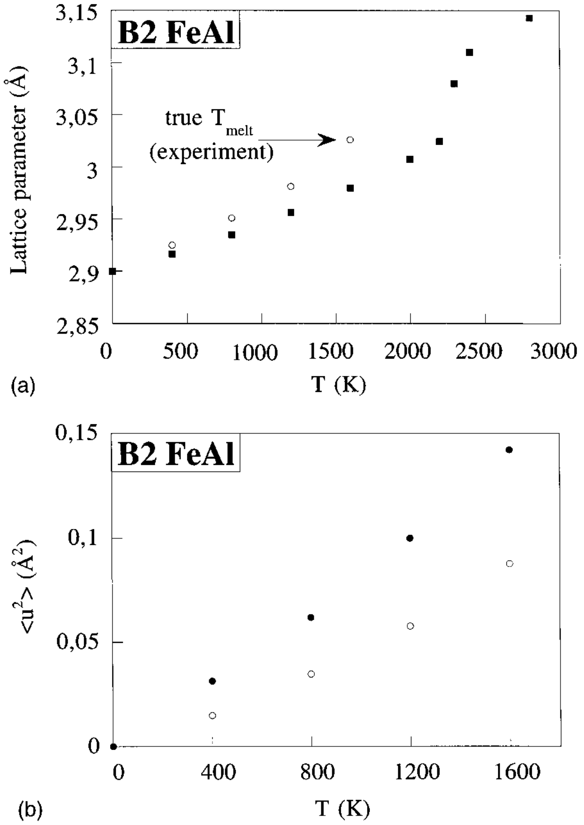

FIG. 4. (a) Thermal expansion, as calculated with our model (full squares) and experimentally measured (Ref. 62); (b) mean square displacements in $B2$ FeAl (Al and Fe atoms in open and full circles, respectively).

d. Antiphase boundary and point defects. The fitting was performed on the 300 mJ/m^2 theoretical value of the $1/2[111](1\bar{1}0)$ antiphase boundary energy, as obtained from first-principles calculations in Ref. 35. To preserve the coherency of our model (fitted on *ab initio* values of elastic constants), and also because experimental results stem from boundaries whose local composition were not known, we preferred such theoretical values to experimental measurements of antiphase boundaries energies at 300 K, also available in the literature[64] and approximately twice lower. After optimization, the better value obtained for this relaxed defect amounted to 370 mJ/m^2.

The point defect energies are defined in the usual way as the difference between the energy of a system containing one isolated defect and that of a reference perfect crystal containing the same number of atoms of each species:

$$E_f^{\text{def}} = E^{\text{def}}(N_{\text{Al}}, N_{\text{Fe}}) - N_{\text{Al}} E^0_{\text{Al}} - N_{\text{Fe}} E^0_{\text{Fe}}, \tag{13}$$

where E^0 stands for the chemical potentials at zero temperature and pressure. Although point defects have been already studied in $B2$ FeAl, no clear picture of their disposition could be drawn up to now. On the Fe-rich side, antistructure Fe atoms are assumed to be predominant, whereas for stoichiometric and Al-rich compounds, more complex defect structures coupling antisite Fe and Fe vacancies are thought to exist. Reliable values for the energies of simple vacancies and antisite atoms have not been firmly determined yet on

TABLE V. Point defect energies (eV) for $B2$ FeAl.

	This work	Mayer *et al.*[c]	Fu *et al.*[a]	Expt.[b]
$E_f^{\nu,\mathrm{Al}}$	2.8	3.71		
$E_f^{\nu,\mathrm{Fe}}$	0.8	1.03	0.97	0.7
$E_f^{a,\mathrm{Al}}$	0.78	1.05	1.04	
$E_f^{a,\mathrm{Fe}}$	0.76	1.03	0.95	

[a] Reference 36.

[b] Reference 63.

[c] Reference 65.

experimental grounds, because such methods do not make it possible to uncorrelate the respective influences of nonindependent defects. *Ab initio* calculations have constituted an appealing way of obtaining plausible values for isolated defect energies. The corresponding results are summed up in Table V, together with the results of the present semiempirical work. On the whole, *ab initio* calculations yield higher values than our semiempirical approach. This discrepancy can partly be attributed to the insufficient size of the cell used in the former calculations. In our work, we had to take into account up to five neighbor shells, while cells used in *ab initio* methods only involve few tens of atoms. This implies that the sizes of cells used in *ab initio* calculations (Ref. 36) are probably not sufficient for the computations to have converged. However, these authors do not find any definite sense of variation of the defect energies when increasing the box size. Thus, if the interaction between the defect studied and its images in the neighboring cells can certainly not be neglected in their work, this cannot be regarded as the only reason for the smaller values of defect energies obtained in the present paper. On the other hand, the ratios between the different kinds of defects are preserved when going from *ab initio* to empirical studies, indicating that the nonindependence between defects merely acts as a scaling factor. Moreover, the agreement between both methods is quite satisfactory, confirming that the Al vacancy is indeed the most expensive defect.

Within the frame of a simple model using the grand canonical formalism on a rigid lattice (no vibrational entropy), concentrations can be easily calculated for each of the four above mentioned independent defects. One obtains for the fractions of α (Al) or β (Fe) sites occupied by the wrong type of atom or by a vacancy

$$x^{\mathrm{Al},\beta}=\frac{\exp(-E_f^{\mathrm{Al},\beta}/kT)}{1+\exp(-E_f^{\mathrm{Al},\beta}/kT)+\exp(-E_f^{\nu,\mathrm{Fe}}/kT)} \quad (14a)$$

$$x^{\nu,\mathrm{Al}}=\frac{\exp(-E_f^{\nu,\mathrm{Al}}/kT)}{1+\exp(-E_f^{\mathrm{Fe},\alpha}/kT)+\exp(-E_f^{\nu,\mathrm{Al}}/kT)} \quad (14b)$$

and similar formulas for $x^{\mathrm{Fe},\alpha}$, $x^{\nu,\mathrm{Fe}}$.

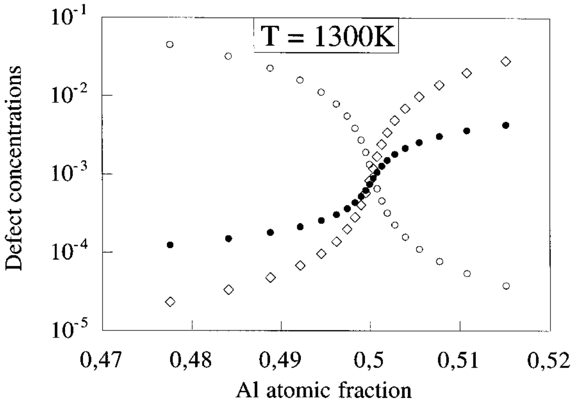

FIG. 5. Independent point-defect concentrations in a rigid-lattice model under zero pressure, as calculated with values of Table V. Squares stand for Al on the Fe (β) sublattice, open circles for Fe on the Al (α) sublattice, and full circles for vacancies on the Fe sublattice. The amount of Al vacancies is found to be almost zero.

From Fig. 5, showing the results at 1300 K under zero pressure, it is clear that the potential discriminates quite sharply between Fe and Al vacancies, the former being indeed the more favorable one, whatever the composition around $x=0.5$. On the Fe-rich side, the predominant defect is antisite Fe, in agreement with previous results (see Ref. 1). For Al-rich compounds, this simple model predicts that off stoichiometry will be allowed for by the simultaneous presence of antisite Al and Fe vacancies, in contradiction with the observations reported above (no antisite Al atoms). On the other hand, in agreement with our work, *ab initio* calculations combined with independent defect models also predict non-negligible amounts of antisite Al atoms. Both antisite defects having nearly equal energies, the negligible amount of Al antisites on the Al-rich side, reported in the literature, is probably to be put down to more stable complexes.

The vacancy concentration for $x=0.5$ is found to be 10^{-3}, which is of the same order of magnitude as the value experimentally determined in a 40 at. % Al alloy (0.2%).[63] However, the latter value must be considered cautiously, since such deviations from stoichiometry are probably accommodated by complex defects. This is confirmed by the work of Fu *et al.*[36] who obtained a divacancy binding energy equal to 0.57 eV, and by that of Paris[66] in the 49.5 at. % Al compound, showing that the proportion of Fe vacancies surrounded by antistructure Fe could certainly not be neglected (up to three antisite Fe were found to occupy the first-nearest neighbor positions of the Fe vacant site). Neumann *et al.*[67] also showed that triple defects should be essential in the $B2$ alloy.

2. Partial energies for alloys containing 25 and 50 at. % Al

Of prime importance to assess the quality of the alloy potential is its ability to predict the amount of energy attached to each species when the local environment (depending on the global concentration) varies. Table VI shows the values of chemical potentials for Fe atomic fractions equal to

TABLE VI. Chemical potentials (eV) under zero temperature and pressure in FeAl and Fe_3Al. Experimental values are deduced from room temperature enthalpy measurements (Ref. 44).

	μ_{Al}		μ_{Fe}	
	Calc.	Expt.	Calc.	Expt.
$B2$	−3.57	−3.65	−4.58	−4.50
$D0_3$	−3.66	−3.80	−4.46	−4.25

TABLE VII. Characteristics of the calculated $D0_3$ phase compared with experimental data. Energies in eV/(3 Fe+1 Al); lattice parameters in Å; elastic constants in 10^{12} dyn cm^{-2}.

	Experimental (300 K)	Extrapolated (0 K)	Calculated (0 K)
E(3 Fe+1 Al)	-17.02^{a}		-17.1
$2a$	5.79^{b}		5.732
C_{11}	1.71^{c}	1.79^{d}	2.62
C_{12}	1.31^{c}	1.31^{d}	1.56
C_{44}	1.32^{c}	1.38^{d}	1.62
$C_{12}-C_{44}$	-0.01	-0.07	-0.06
$E(D0_3)-E(L1_2)$			-1.41

[a] Reference 44.
[b] Reference 45.
[c] Reference 46.
[d] Reference 68.

0.5 and 0.75, as calculated with the present interatomic potential, for comparison with experiments. To get estimates of the real partial free energies, we made use of the well-known rule of intersection between each tangent and $x=0$ or $x=1$ axes. Our model correctly describes the trend of increasing chemical potential difference μ_{Fe}-μ_{Al}, when shifting from $D0_3$ to $B2$ structure. Although deviation from experiment is more pronounced for the $D0_3$ structure (a logical result since no particular endeavor was made upon a good decription of this structure), the discrepancy never exceeds 10%. Finally, if one considers the limited accuracy of experimental data, the reasonable agreement with our results incites to be quite confident as regards future evaluations of defect structures.

3. $D0_3$ properties

As previously recalled, it is essential to know precisely the range of compositions in which an alloy model is valid. Results of a small number of tests to assess this validity for Fe_3Al are reported in Table VII. The agreement with experience is good for both alloy formation energy (as discussed in the previous section) and lattice parameter. Elastic constants were evaluated numerically, as second-order derivatives of the energy. Whereas the system is still at equilibrium after homogeneous displacements corresponding to C' and B, calculation of C_{44} *a priori* requires taking into account the atomic relaxations induced by performing a shear displacement. However, results before and after relaxations only disagree by a few percent. Table VII gives the results relative to the relaxed state, together with experimental values at 300 K and extrapolated values at 0 K. Apart from C_{11}, for which the discrepancy amounts to 30%, the agreement between our results (calculated at 0 K) and these extrapolated constants is very good, especially if one considers that they were not taken into account in the fitting procedure. Moreover, as for the $B2$ structure, the negative difference $C_{12}-C_{44}$ in Fe_3Al is predicted, as well as its almost zero magnitude.

The stability of the $D0_3$ structure was tested against that of the also very common $L1_2$ (A_3B cfc-based ordered) structure. As Table VII shows, $D0_3$ was found to be energetically more favorable. This point is worth emphasizing, since closely related potentials[32–34] (except for the noncentral part) enabled a good description of the Ni-Al system and especially of Ni_3Al, which however exhibits a $L1_2$ structure and whose angular distribution of neighboring atoms of each type is completely different from that in the $D0_3$ structure. The noncentral part being identically zero for all concerned perfect structures, it cannot be regarded as responsible for these various behaviors. The absence of relation between explicitly angular interactions and favoring of any particular monocrystalline atomic arrangement is consistent with the well-known property that before all, such interactions cannot be omitted in the study of defects, with reduced symmetry. In our case, iron seems to be mostly responsible for the atomic arrangement, since whatever the atomic Al percentage, it imposes a bcc-based structure, the lattice parameter of which is almost insensitive to this percentage. Apart from the atomic arrangement, iron plays probably an important role in elastic properties: the negative Cauchy difference is probably to be put down to the simple cubic bonds between Fe atoms in $B2$ FeAl. However, we have not performed any calculation to check this point. An *ab initio* approach would be doubtlessly preferred, because the validity of the parameter α in the present potential cannot be ensured for pure Fe in cubic structure.

Finally, as regards the competition between the $B2$ and $B32$ on the one hand, and between $D0_3$ and $L1_2$ on the other hand, the model yields two very distinct behaviors: whereas the $D0_3-L1_2$ energy difference amounts to -0.35 eV/atom, only -0.05 eV/atom separate the $B2$ and $B32$ structures. This indicates that the latter might be quite easily stabilized under particular conditions. A diffuse neutron scattering study[69] revealed the presence of the $B32$ phase at temperatures below 650 K, raising the question of whether $B32$ is not the true ground state. The $B2$ phase would then be favored only for kinetic reasons. Using x-ray diffraction, other authors[70] have also shown that the $B32$ phase exists in quenched materials, in relation with antiphase domains. If not the ground state, this phase could thus at least appear on a very local scale due to the stresses developed in the crystal on rapid cooling. Anyway, the present empirical model plaids (at least qualitatively) for a strong competition between $B2$ and $B32$. A thorough calculation of the Gibbs free energy of both phases for various temperature and stress conditions may therefore be very helpful in understanding equilibrium properties and (indirectly) kinetic effects.

IV. CONCLUSIONS

The key purpose of this work consisted in devising a unique potential applicable to very different kinds of metallic materials, namely a fcc normal metal, a bcc transition metal, and a mixture of both characterized by highly directional effects. Because of the practical interest of understanding the very intricate mechanical properties of Fe-Al systems, properties wholly controlled by interfacial segregation phenomena, this potential had to faithfully reproduce the elastic and chemical alloy behaviors. Especially if one confines to zero-temperature properties and well-defined compositions corresponding to the strongly ordered $B2$ and $D0_3$ phases, the result proves to be satisfactory and will probably make it possible to calculate room-temperature segregation properties and thus draw comparisons with the behavior of thoroughly studied Ni-Al systems.

Due to the reduced number of models available at present for alloys, and particularly for highly ordered ones, the models presented in Refs. 32–34 constitute precious references for future comparisons concerning bulk as well as defect properties. The present potential for $B2$ FeAl alloys proved to be quite satisfactory in the description of pure elements and of this compound, characterized by strong directional bonds. The method, consisting first to fit two separate models for Fe and Al and then to determine a cross potential and angular parameters specific to the $B2$ alloy, allowed for the negative Cauchy discrepancy. The potential giving quite plausible values for elastic and chemical properties for $B2$ as well as $D0_3$ structures, it should make it possible to tackle the study of various properties in iron-rich FeAl. In particular, one can reasonably be confident of its ability to study the interfacial segregation phenomena responsible for the high complexity of Fe-Al mechanical properties.

ACKNOWLEDGMENTS

We are indebted to M. Biscondi, A. Fraczkiewicz, and V. Pontikis for helpful discussions. One of us (R.B.) also wishes to thank M. Biscondi and T. Magnin for providing him the opportunity of collaboration with the L.S.I.

---

[*] Present address: Laboratoire des Solides Irradiés, CEA-CEREM, URA CNRS 1380, Ecole Polytechnique, 91128 Palaiseau CEDEX, France.

[1] *Intermetallic Compounds: Principles and Practice*, edited by J. H. Westbrook and R. L. Fleischer (Wiley, New York, 1994).

[2] R. L. Fleischer, D. M. Dimiduk, and H. A. Lipsitt, Annu. Rev. Mater. Sci. **19**, 231 (1989).

[3] E. S. Machlin, Acta Metall. **22**, 95 (1974).

[4] Z. A. Matysina, O. S. Pogorelova, S. Y. Zaginaichenko, and D. V. Schur, J. Phys. Chem. Solids **56**, 9 (1995).

[5] R. C. Crawford, Philos. Mag. **35**, 567 (1977).

[6] C. Bichara and G. Inden, Scr. Metall. Mater. **25**, 2607 (1991).

[7] F. Schmid and K. Binder, J. Phys. C **4**, 3569 (1992).

[8] R. Besson, A. Fraczkiewicz, and M. Biscondi, J. Phys. (France) IV **6**, C2-47 (1996).

[9] I. Baker (unpublished).

[10] M. S. Daw, Phys. Rev. B **39**, 7441 (1989).

[11] V. Rosato, M. Guillopé, and B. Legrand, Philos. Mag. A **59**, 321 (1989).

[12] D. J. Oh and R. A. Johnson, J. Mater. Res. **3**, 471 (1988).

[13] G. J. Ackland, G. Tichy, V. Vitek, and M. W. Finnis, Philos. Mag. A **56**, 735 (1987).

[14] M. W. Finnis and J. E. Sinclair, Philos. Mag. A **50**, 45 (1984).

[15] A. G. Marinopoulos, V. Vitek, and A. E. Carlsson, Philos. Mag. A **72**, 1311 (1995).

[16] M. W. Finnis, A. T. Paxton, D. G. Pettifor, A. P. Sutton, and Y. Ohta, Philos. Mag. A **58**, 143 (1988).

[17] A. P. Sutton, M. W. Finnis, D. G. Pettifor, and Y. Ohta, J. Phys. C **21**, 35 (1988).

[18] A. E. Carlsson, in *Many-Atom Interactions in Solids*, edited by R. M. Nieminen, M. J. Puska, and M. J. Manninen (Springer-Verlag, Berlin, 1990), p. 257.

[19] J. C. Slater and G. F. Koster, Phys. Rev. **94**, 1498 (1954).

[20] R. H. Brown and A. E. Carlsson, Phys. Rev. B **32**, 6125 (1985).

[21] S. M. Foiles, Phys. Rev. B **48**, 4287 (1993).

[22] F. H. Stillinger and T. A. Weber, Phys. Rev. B **31**, 5262 (1985).

[23] R. Biswas and D. R. Hamann, Phys. Rev. Lett. **55**, 2001 (1985).

[24] M. I. Baskes, J. S. Nelson, and A. F. Wright, Phys. Rev. B **40**, 6085 (1989).

[25] M. I. Baskes, Phys. Rev. Lett. **59**, 2666 (1987).

[26] R. Pasianot, D. Farkas, and E. J. Savino, Phys. Rev. B **43**, 6952 (1991).

[27] H. Kanzaki, J. Phys. Chem. Solids **2**, 24 (1957).

[28] S. M. Foiles, M. I. Baskes, and M. S. Daw, Phys. Rev. B **33**, 7983 (1986).

[29] H. Rafii-Tabar and A. P. Sutton, Philos. Mag. Lett. **63**, 217 (1991).

[30] C. Rey-Losada, M. Hayoun, and V. Pontikis, in *Materials Theory and Modelling*, edited by J. Broughton, P. D. Bristowe, and J. M. Newsam, MRS Symposia Proceedings No. 291 (Materials Research Society, Pittsburgh, 1993), p. 549.

[31] A. M. Guellil and J. B. Adams, J. Mater. Res. **7**, 639 (1992).

[32] A. F. Voter and S. P. Chen, in *Characterization of Defects in Materials*, edited by R. W. Siegel, J. R. Weertman, and R. Sinclair, MRS Symposia Proceedings No. 82 (Materials Research Society, Pittsburgh, 1987), p. 175.

[33] M. Ludwig and P. Gumbsch, Modelling Simul. Mater. Sci. Eng. **3**, 533 (1995).

[34] S. Rubini and P. Ballone, Phys. Rev. B **48**, 99 (1993).

[35] C. L. Fu and M. H. Yoo, Acta Metall. Mater. **40**, 703 (1992).

[36] C. L. Fu, Y. Y. Ye, and M. H. Yoo, in *High-Temperature Ordered Intermetallic Alloys V*, edited by I. Baker *et al.*, MRS Symposia Proceedings No. 288 (Materials Research Society, Pittsburgh, 1993), p. 21.

[37] P. A. Schultz and J. W. Davenport, J. Alloys Compd. **197**, 229 (1993).

[38] A. F. Voter, in *Intermetallic Compounds* (Ref. 1), p. 77.

[39] D. G. Pettifor and M. Aoki, Philos. Trans. R. Soc. London Ser. A **334**, 439 (1991).

[40] D. G. Pettifor, M. Aoki, P. Gumbsch, A. P. Horsfield, D. Nguyen Manh, and V. Vitek, Mater. Sci. Eng. A **192–193**, 24 (1995).

[41] J. Moriarty, Phys. Rev. B **42**, 1609 (1990).

[42] R. Eibler and A. Neckel, J. Phys. F **10**, 2179 (1980).

[43] C. Kittel, *Introduction to Solid State Physics* (Wiley, New York, 1966).

[44] R. Hultgren, P. D. Desai, D. T. Hawkins, M. Gleiser, K. K. Kelley, and D. D. Wagman, *Selected Values of the Thermodynamic Properties of Binary Alloys* (American Society for Metals, Metals Park, OH, 1973).

[45] W. B. Pearson, *Handbook of Lattice Spacings and Structures of Metals* (Pergamon, London, 1964).

[46] G. Simmons and H. Wang, *Single Crystal Elastic Constants and Calculated Aggregate Properties* (M.I.T. Press, Boston, 1971).

[47] J. H. Rose, J. R. Smith, F. Guinea, and J. Ferrante, Phys. Rev. B **29**, 2963 (1984).

[48] C. H. Bennett, *Diffusion in Solids: Recent Developments* (Academic, New York, 1975).

[49] A. R. Miedema, Z. Metallkd. **69**, 287 (1978).

[50] B. N. Brockhouse and A. T. Stewart, Rev. Mod. Phys. **30**, 236 (1958).

[51] V. J. Minkiewicz, G. Shirane, and R. Nathans, Phys. Rev. **162**, 528 (1967).

[52] R. Stedman, L. Almqvist, and G. Nilsson, Phys. Rev. **162**, 549 (1967).

[53] *Computer Simulation in Materials Science: Interatomic Potentials, Simulation Techniques and Applications*, Vol. 205 of *NATO Advanced Study Institute, Series E: Applied Sciences*, edited by M. Meyer and V. Pontikis (Kluwer, Dordrecht, 1991).

[54] Z. S. Basinski, W. Hume-Rothery, and A. L. Sutton, Proc. R. Soc. London Ser. A **229**, 459 (1955).

[55] R. W. James, G. W. Brindley, and R. E. Wood, Proc. R. Soc. London Ser. A **125**, 401 (1929).

[56] P. Debrunner and R. J. Morisson, Rev. Mod. Phys. **36**, 463 (1964).

[57] F. A. Lindemann, Phys. Z. **11**, 609 (1910).

[58] J. N. Shapiro, Phys. Rev. B **1**, 3982 (1970).

[59] J. J. Gilvarry, Phys. Rev. **102**, 308 (1956).

[60] A. E. Carlsson and P. E. Meschter, in *Intermetallic Compounds* (Ref. 1), p. 55.

[61] A. M. Robertson, J. Phys. C **3**, 8181 (1991).

[62] W. D. Porter and P. J. Maziasz, Scr. Metall. Mater. **29**, 1043 (1993).

[63] J. Rieu and C. Goux, Mem. Scient. Rev. Metall. **66**, 869 (1969).

[64] R. C. Crawford and L. F. Ray, Philos. Mag. **35**, 549 (1977).

[65] J. Mayer, C. Elsässer, and M. Fähnle, Phys. Status Solidi B **191**, 283 (1995).

[66] D. Paris, Ph.D. thesis, Ecole des Mines, Saint-Etienne, France, 1979.

[67] J. P. Neumann, Y. A. Chang, and C. M. Lee, Acta Metall. **24**, 593 (1976).

[68] H. J. Leamy, E. D. Gibson, and F. X. Kayser, Acta Metall. **15**, 1827 (1967).

[69] W. Schweika, in *Neutron Scattering for Materials Science*, edited by S. M. Shapiro, S. C. Moss, and J. D. Jorgensen, MRS Symposia Proceedings No. 166 (Materials Research Society, Pittsburgh, 1990), p. 249.

[70] Z. Q. Gao and B. Fultz, Philos. Mag. B **67**, 787 (1993).